Journal of Alloys and Compounds 509 (2011) 2105–2110

Contents lists available at ScienceDirect

Journal of Alloys and Compounds

journal homepage: www.elsevier.com/locate/jallcom

The effects of Ni and Mg_2Ni interlayer on hydrogenation properties of Pd sandwiched Mg films

Pragya Jain[a,*], Ankur Jain[a], Devendra Vyas[a], Reena Verma[a], S.A. Khan[b], I.P. Jain[a]

[a] Centre for Non-Conventional Energy Resources, University of Rajasthan, Jaipur 302055, India
[b] Inter University Accelerator Centre, New Delhi 110 067, India

ARTICLE INFO

Article history:
Received 17 September 2010
Received in revised form 20 October 2010
Accepted 27 October 2010
Available online 4 November 2010

Keywords:
Hydrogen storage materials
Mg thin films
Hydrogen content
ERDA

ABSTRACT

The scope of present study is to investigate and compare the areal hydrogen concentration of Pd/Mg/Ni/Pd and Pd/Mg/Mg_2Ni/Pd films with the Pd/Mg/Pd base system using Elastic Recoil Detection Analysis (ERDA) technique. Metals were deposited on Si substrate by thermal evaporation and electron gun evaporation technique followed by hydrogenation for 2 h at 150 °C and 2 bar hydrogen pressure. ERDA study reveals that Pd/Mg/Ni/Pd and Pd/Mg/Mg_2Ni/Pd films absorb 7.08×10^{17} and 1.68×10^{18} hydrogen atoms/cm^2, respectively, in comparison to 4×10^{17} atoms/cm^2 absorbed by base system. The influence of Ni and Mg_2Ni interlayer on the hydrogen storage properties of base system were investigated by changes in structural and surface topographical properties using XRD and AFM techniques, respectively. These results strongly supports the ERDA findings, clearly shows that the addition of Ni or Mg_2Ni layers to base system enhances its hydrogenation and decreases the oxygen content. The high hydrogen content in Mg/Mg_2Ni bilayer can be explained by the formation of MgH_2 and Mg_2NiH_4 phases.

1. Introduction

Magnesium (Mg) based materials have attracted extensive attention as light weight hydrogen storage materials in the future hydrogen economy due to the high hydrogen storage capacity, 7.6 wt% of MgH_2, light weight, low cost and abundance on earth crust. Moreover, the release of hydrogen from Mg occurs via a simple one step process without any by-products [1–3]. However, there are certain obstacles of pure Mg which prevents its on-board application as storage material, e.g.

(a) High thermodynamic stability of hydride causing high temperature hydrogen desorption.
(b) Poor hydriding/dehydriding kinetics due to low dissociation rate of hydrogen.
(c) Slow diffusion of hydrogen in magnesium hydride phase.
(d) High susceptibility of Mg to oxidation.

During the past few years substantial improvement in the sluggish kinetics for hydrogen storage has been achieved by several methods [4–6]. The most effective methods are due to the structural modification of these systems and by introducing proper additives, e.g. Ni in Mg leads to the formation of Mg–Ni alloys like Mg_2Ni in which Ni helps in dissociation of hydrogen molecules resulting hydrogen atom diffusion and reacting with the metal atoms to form MgH_2 and Mg_2NiH_4 [7–9]. Recently, it has been shown that addition of 6–10 mol% Mg_2Ni to MgH_2 leads to reduction in the onset temperature from 330 °C to 190 °C with storage capacity of 6 wt% demonstrating improved thermodynamics and kinetics by forming nano-composite of Mg based alloys with suitable catalysts [10].

One of the ways to form nano-composite by thin film preparation as one can control film thickness, composition, interface and structural order. Moreover, the co-operative phenomena and the spill over effects can be induced by synthesis of sandwich structured films, leading to an improved kinetics [11–13].

Present work investigates effect of Ni and Mg_2Ni interlayer on the hydrogen storage capacity of Mg thin films sandwiched between Pd layers. Systematic study has been undertaken for hydrogen content, structural properties and morphological variations by ERDA, XRD and AFM, respectively.

2. Experiment

Thin film samples are prepared on Si [1 0 0] substrate by vapor deposition in a HV chamber, equipped with 3 kW electron gun, two thermal deposition units, two shutters and quartz crystal microbalance at 10^{-7} mbar vacuum. For the base sample Pd/Mg/Pd, a 150 nm Mg layer was thermally deposited at rate 0.15 nm/s and sandwiched between 20 nm layers of Pd deposited at 0.1 nm/s rate by

* Corresponding author. Tel.: +91 9784584616; fax: +91 1412711049.
E-mail addresses: pragya.2604@gmail.com (P. Jain), ipjain46@gmail.com (I.P. Jain).

0925-8388/$ – see front matter © 2010 Elsevier B.V. All rights reserved.
doi:10.1016/j.jallcom.2010.10.151

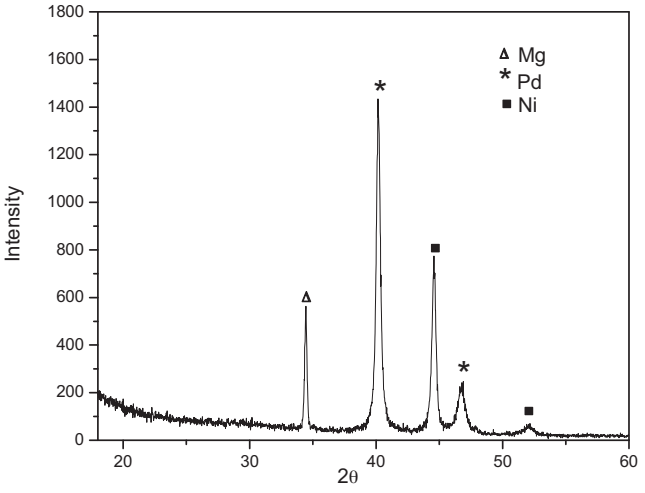

Fig. 1. XRD pattern of as-deposited Pd sandwiched Mg/Ni film.

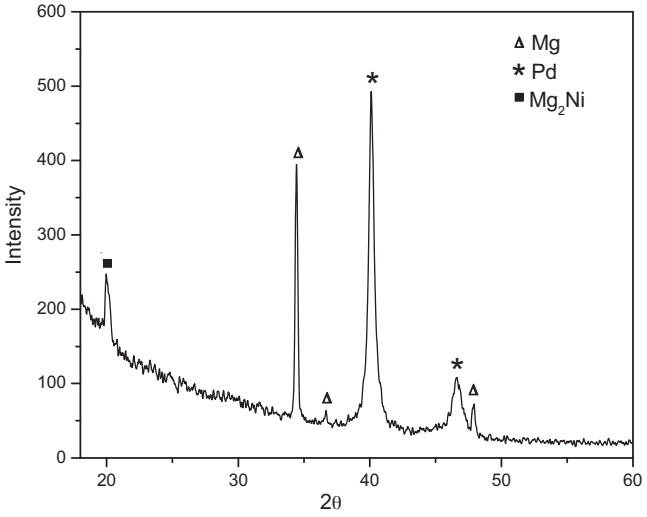

Fig. 2. XRD pattern of as-deposited Pd sandwich Mg/Mg_2Ni bilayer film.

e-gun. The sandwiched structure ensures protection against oxidation from both the surface and substrate side in addition to hydrogen dissociation. A 50 nm Ni layer deposited at a rate of 0.1 nm/s replaces 50 nm Mg layer to form Pd/Ni/Mg/Pd film while $Pd/Mg_2Ni/Mg/Pd$ is prepared by substituting 50 nm Mg by Mg_2Ni alloy layer. The Mg_2Ni alloy is prepared by co-evaporation of Mg at 0.2 nm/s rate and Ni at 0.019 nm/s rate from thermal and e-gun sources respectively.

The deposited samples were transferred into the stainless steel hydrogenation set-up as designed to work under 10^{-5} mbar vacuum followed by exposing to hydrogen gas at 2 bar pressure and 150 °C temperature for 2 h. Three cycles of hydrogen absorption/desorption were performed to ensure complete hydrogenation of the films.

The structures of the as-deposited and hydrogenated samples were studied by GIXRD technique using monochromated Cu Kα radiation with model Brucker DX 8-Advance. The spectra were recorded in the 2θ range of 15–55° with scan speed of 0.5°/min and step width of 0.02°. The surface morphology of all the samples have been investigated by AFM (Nanoscope IIIE model from Digital Instruments, USA), in contact mode at room temperature. The scan area and rate were kept as 5×5 μm and 1.526 Hz, respectively.

After hydrogenation, Elastic Recoil Detection Analysis (ERDA) measurements were performed at Material Science beam line in IUAC, New Delhi using 120MeV Ag^{9+} beam to determine the areal concentration of hydrogen (N_H in atoms cm^{-2}) and other light elements like oxygen. The beam of spot size 1×1 mm^2 was impinged on the sample kept at an angle of 20° under a base pressure of 4.5×10^{-6} mbar. The H-recoils from the film were detected in a silicon surface barrier detector (SSBD) kept at 30° recoil angle preceded by a 1.5 μm polypropylene stopper foil in front of it to stop other recoils. Other recoils like O were detected in Isobutene gas filled detector placed at 45° recoil angle. The areal concentration of hydrogen (H) (N_H atoms $cm^{-2} \pm 5\%$) atoms were calculated using the following equation:

$$N_H = \frac{Y \sin\alpha}{N_p(d\sigma/d\Omega)\Omega} \quad (1)$$

where Y is the integral counts obtained by the recoil energy spectra, α is the target tilt angle, Ω is the solid angle subtended by the detector and $d\sigma/d\Omega$ is the Rutherford recoil cross section. The fluence-dependent N_H was estimated from the on-line data, taken in event-by-event mode [14].

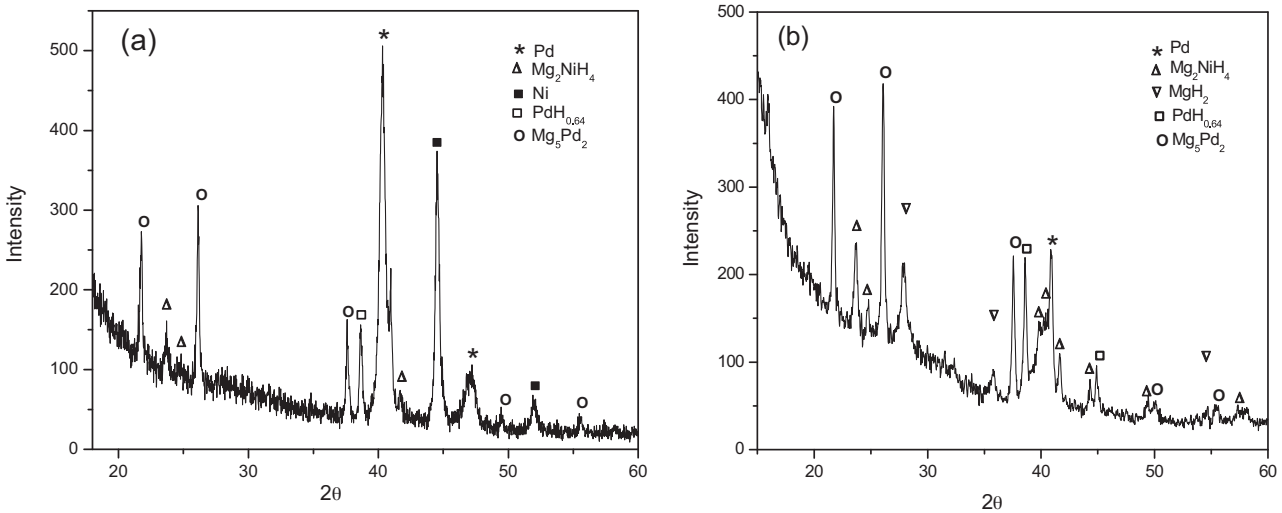

Fig. 3. XRD pattern of Pd sandwich (a) Mg/Ni and (b) Mg/Mg_2Ni bilayer films undergone hydrogenation at 150 °C at 2 bar H_2 pressure for 2 h.

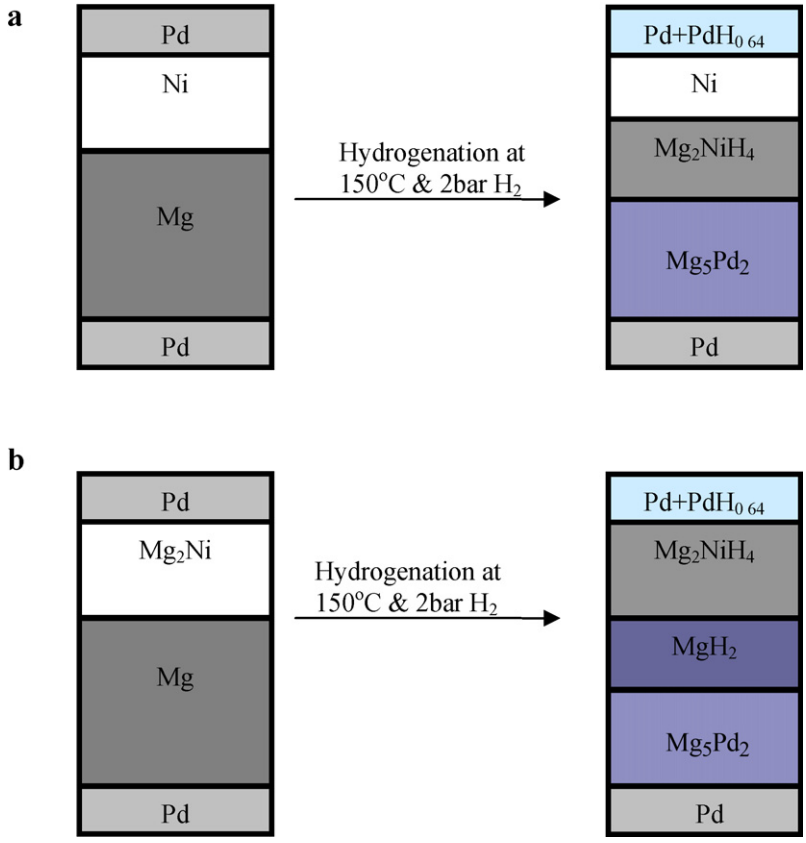

Fig. 4. Schematic diagram representing the possible reaction occurring in (a) Pd/Mg/Ni/Pd and (b) Pd/Mg/Mg_2Ni/Pd films during hydrogenation.

3. Results and discussions

3.1. Structural properties of thin film system

Fig. 1 shows XRD pattern of as-deposited Pd/Mg/Ni/Pd film with peaks at around 34.4°, characteristic of Mg [0 0 2] and peaks at 44.57° and 52.06° corresponding to Ni [1 1 1] and [2 0 0] orientations. Fig. 2 shows the XRD pattern of Pd/Mg/Mg_2Ni/Pd sample with peak at around 20° characteristic of Mg_2Ni [1 0 0] along with three peaks corresponding to h-Mg with [0 0 2], [1 0 1] and [1 0 2] orientations. In these figures, peaks at 40.19° and 46.84° correspond to Pd [1 1 1] and [2 0 0] peaks revealing the formation of nano-crystalline microstructures of the deposited elements in multilayered films. The absence of any peak corresponding to oxide suggests that Pd capping at both top and bottom surfaces prevents oxidation of Mg. Fig. 3(a) and (b) presents the XRD spectra of hydrogenated Pd/Mg/Ni/Pd (HD1) and Pd/Mg/Mg_2Ni/Pd (HD2) samples showing the presence of small amount of Mg_2NiH_4 along with $PdH_{0.64}$ corresponding to HD1 sample suggesting interfacial reaction of Mg–Ni to form Mg_2Ni phase during annealing, which subsequently transforms into hydride phase upon hydrogen exposure. However, the quantitative amount of Mg_2NiH_4 phase is less compared to Mg–Pd alloy phase formed as a result of high reactivity between Mg and Pd in comparison to Mg and Ni similar to several studies [15]. The existence of pure Ni peak in Fig. 3(a) even after hydrogenation further supports the formation of small amount of Mg_2NiH_4 in HD1. Most of the Pd also remains unhydrogenated as evident from the presence of an intense peak of pure Pd, which is in agreement with several reports [16]. Additionally Pd peak broadening is noticed which is an indication of decay of crystallite size of Pd from 44 nm to 35 nm calculated by Debye Scherer formula may be due to several hydrogenation cycles, since Pd provides diffusion path for H_2. However, the diffraction peak of Ni shown in Fig. 3a becomes sharper than that in Fig. 1 with crystallite size becoming 51 nm from 45 nm which may be due to growth of Ni crystal under hydrogenation temperature [17]. Sample HD2 contains peaks corresponding to Pd, $PdH_{0.64}$ and Mg_5Pd_2, nearly similar to those observed in HD1 along with the existence of Mg_2Ni promoting the direct formation of Mg_2NiH_4 in large amount. Moreover, the ternary hydride facilitates the diffusion path for hydrogen to react with Mg and thus form significant amount of MgH_2. Fig. 4 represents the schematic diagrams of possible reaction mechanism during hydrogenation of both the samples.

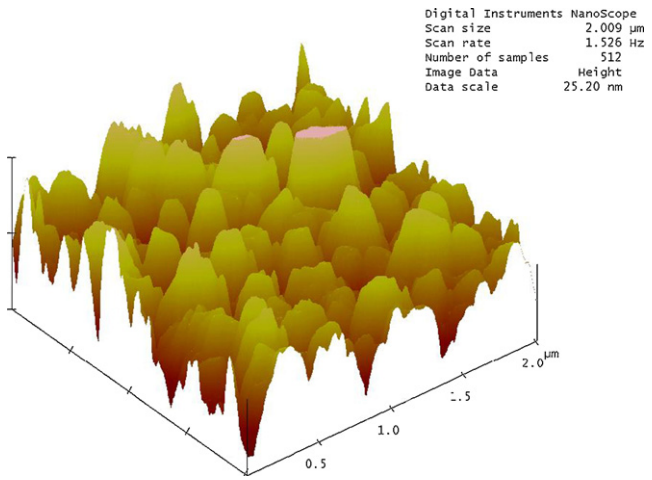

Fig. 5. AFM image of as-deposited Pd sandwich Mg/Ni bilayer film.

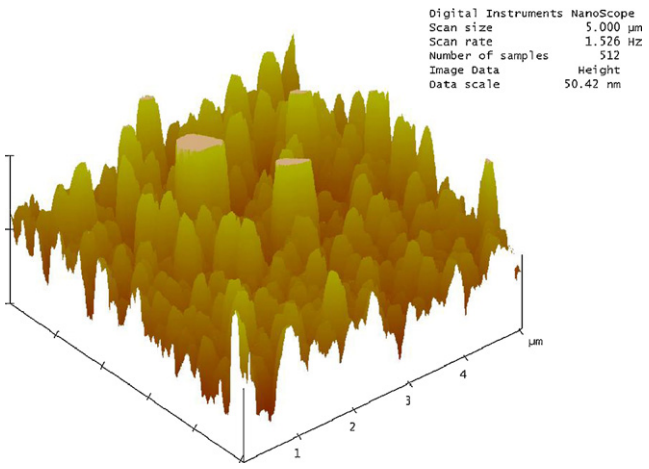

Fig. 6. AFM image of as-deposited Pd sandwich Mg/Mg_2Ni bilayer film.

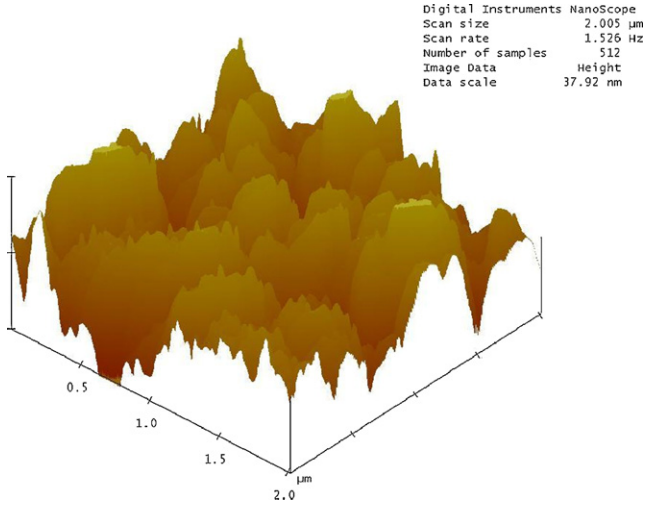

Fig. 7. AFM image of hydrogenated Pd/Mg/Ni/Pd film.

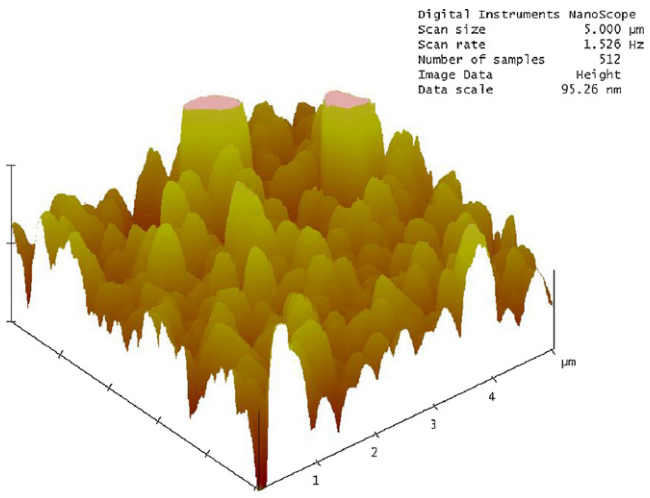

Fig. 8. AFM image of hydrogenated Pd/Mg/Mg_2Ni/Pd film.

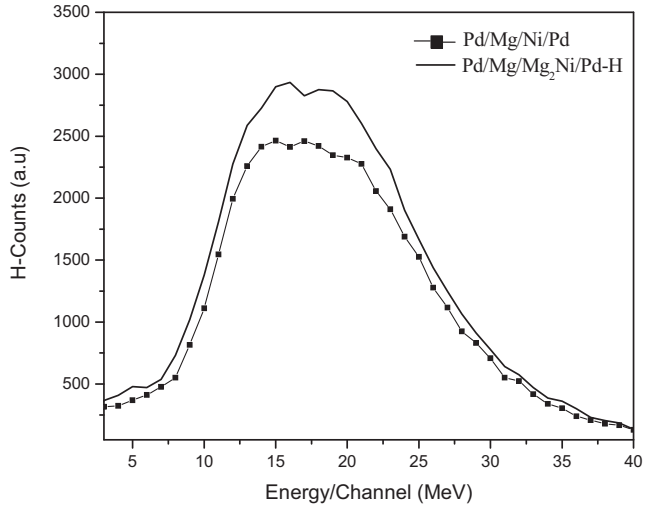

Fig. 9. ERDA spectra of hydrogenated Pd/Mg/Ni/Pd (dotted line) and Pd/Mg/Mg_2Ni/Pd (solid line) film taken at first minute of ERDA measurement.

3.2. Morphological properties of thin films

AFM surface analysis technique provides information regarding the structural transformations in thin films on hydrogenation.

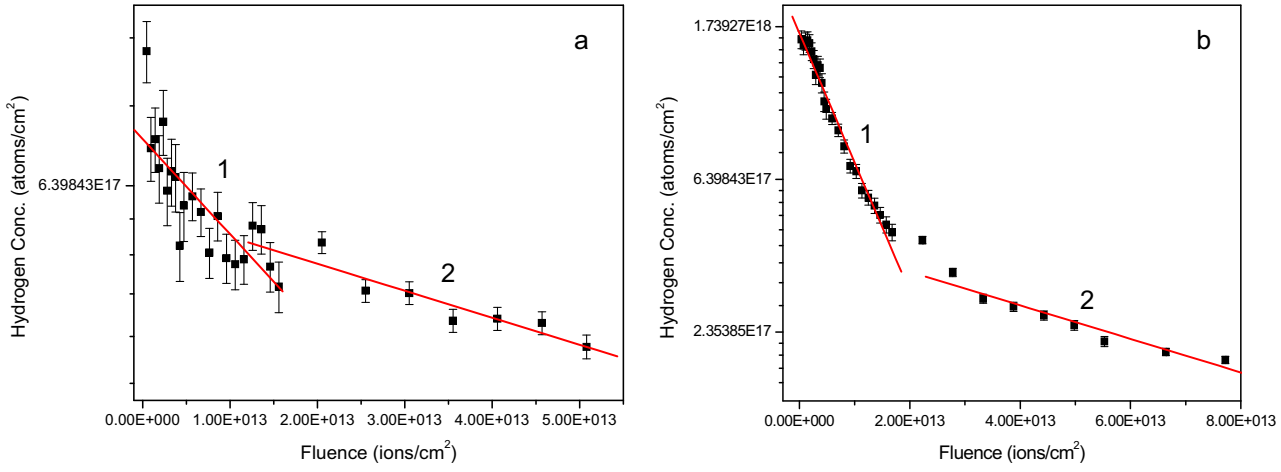

Fig. 10. Variation of hydrogen concentration with fluence of Ag^{9+} 120 MeV ion beam irradiation on hydrogenated (a) Pd/Mg/Ni/Pd and (b) Pd/Mg/Mg_2Ni/Pd films. Solid lines (red) are linear fits of regions 1 and 2 (see text). Error bars show statistical error in the calculated regions. (For interpretation of the references to color in this figure legend, the reader is referred to the web version of the article.)

Table 1
Particle size and roughness calculation from AFM images of as-deposited and hydrogenated samples.

Sample	Particle size (nm)	Roughness (nm)
Pd/Mg/Ni/Pd	361.33	18.844
Pd/Mg/Ni/Pd–H	351.56	27.570
Pd/Mg/Mg2Ni/Pd	160.89	17.301
Pd/Mg/Mg2Ni/Pd–H	140.96	30.793

Figs. 5 and 6 shows the AFM images of as-deposited Pd/Mg/Ni/Pd and Pd/Mg/Mg_2Ni/Pd films and Figs. 7 and 8 displays their corresponding hydrides. The images of as-deposited samples suggest that films have columnar structure with grain boundaries providing path for hydrogen penetration from surface to bulk. Three cycles of hydrogenation at 150 °C and 2 bar H_2 pressure, causes disintegration of particles leading to enhancement in film roughness. Table 1 summarizes the variations in average particle size and mean roughness for the samples. The experimental error in these calculations is of the order of 2 nm.

3.3. Hydrogen content in thin films

The ERDA spectrum of hydrogenated Pd/Mg/Ni/Pd and Pd/Mg/Mg_2Ni/Pd films taken during the first minute of the ERDA measurements is shown in Fig. 9 in which the area under the hydrogen recoil spectra is used to obtain the hydrogen concentration N_H (atoms/cm^2) in the samples at a particular time during experiment [18]. Using equation (1) the amount of hydrogen absorbed by the films N_H under 150 °C and 2 bar H_2 pressure is calculated for different ion dose values. Fig. 10(a) and (b) represents the plot of N_H atoms/cm^2 v/s incident ion fluence (ions/cm^2) after hydrogenation for both the films. The decrease in the hydrogen content is due to H loss on ion irradiation during ERDA analysis [18]. The data are fitted using equation:

$$N_H = N_O \exp(-\sigma\phi), \quad (2)$$

where N_O is the initial concentration of hydrogen, atoms/cm^2, σ is the hydrogen release cross section (cm^2) and ϕ is the ion fluence (ions/cm^2) [19].

The two slopes indicate that after certain fluence, the overlapping of ion damaged zones occurs, causing a change in the value of cross-section in agreement with the model proposed by Mittal et al. [19].

To determine the initial hydrogen concentration in the hydrogenated films, the graphs were extrapolated to zero ion doses as explained by Singh et al. [20]. ERDA result provides the values of areal hydrogen content equal to 7.08×10^{17} and 1.68×10^{18} atoms/cm^2 for HD1 and HD2 samples which are higher than the value reported for Pd/Mg/Pd system in Table 2. This increment in the hydrogen content could be explained as:

(i) The first reason responsible for the increment in hydrogen content can be the varying amount of oxygen content in the three samples, summarized in Table 2. The ERDA plots for O-content in hydrogenated Pd/Mg/Pd, Pd/Mg/Ni/Pd and Pd/Mg/Mg_2Ni/Pd films are also shown in Fig. 11(a)–(c), respectively. It is clear from the above data that base system (Pd/Mg/Pd) has high O-content in comparison to the other two systems which is due to migration of Mg atoms to the surface of the film as expected after three hydrogen cycles, leading to the formation of amorphous MgO and thus preventing hydrogen to diffuse into Mg matrix. Besides, the insertion of Ni and Mg_2Ni layer reduces the interaction between Mg and O resulting in enhanced hydrogen content.

(ii) Second reason may be associated with the presence of different hydriding phases in the three systems. XRD results show the existence of only one hydride phase, i.e. MgH_2 in Pd/Mg/Pd and Mg_2NiH_4 in Pd/Mg/Ni/Pd are responsible for hydrogen content. While Pd/Mg/Mg_2Ni/Pd film shows the presence of two hydrid-

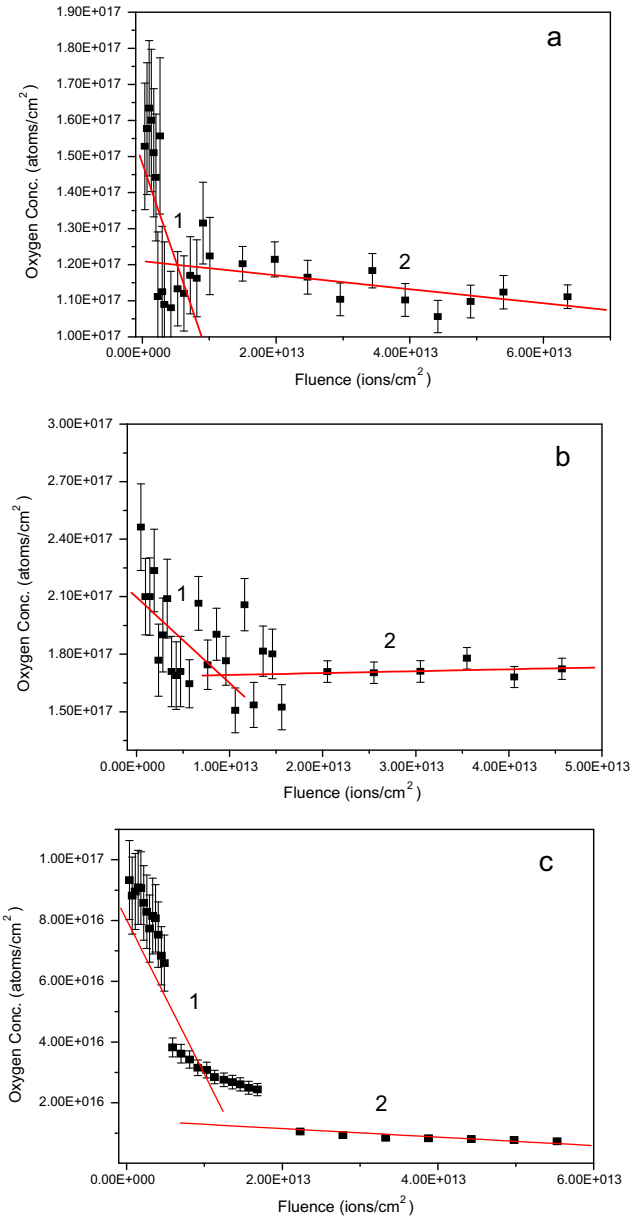

Fig. 11. Variation of oxygen concentration with fluence of Ag^{9+} 120 MeV ion beam irradiation on hydrogenated (a) Pd/Mg/Pd, (b) Pd/Mg/Ni/Pd and (c) Pd/Mg/Mg_2Ni/Pd films. Solid lines (red) are linear fits of regions 1 and 2 (see text). Error bars show statistical error in the calculated regions. (For interpretation of the references to color in this figure legend, the reader is referred to the web version of the article.)

Table 2
ERDA measurements showing areal hydrogen and oxygen content in films after hydrogenation at 150 °C and 2 bar H_2 pressure for 2 h.

Sample	Areal H-content (atoms/cm^2)	Areal O-content (atoms/cm^2)
Pd/Mg/Pd–H	4.00×10^{17}	2.83×10^{17}
Pd/Mg/Ni/Pd–H	7.08×10^{17}	1.68×10^{17}
Pd/Mg/Mg_2Ni/Pd–H	1.68×10^{18}	9.30×10^{16}

ing phases MgH_2 and Mg_2NiH_4 results in best hydrogen content in this system, as determined by ERDA.

4. Conclusion

This study shows the effect of Ni and Mg_2Ni layer addition on the hydrogen storage properties of Pd sandwiched Mg thin films which after deposition are submitted to thermal treatment under 2 bar H_2 pressure at 150 °C for 2 h to promote metal to hydride phase transition. XRD studies supported by ERDA data shows the formation of MgH_2 and Mg_2NiH_4 phases with 1.68×10^{18} hydrogen atoms/cm^2 in Mg/Mg_2Ni film as compared to Mg_2NiH_4 phase with 7×10^{17} hydrogen atoms/cm^2 in Mg/Ni film. We suggest that under given temperature conditions only a small amount of hydrogen absorbing Mg_2Ni phase is formed at Mg/Ni interface of Pd/Mg/Ni/Pd system, while a large amount of Ni remains unreacted and Mg reacts with Pd to form Mg_5Pd_2 alloy. This may be the possible reason responsible for low hydrogen content in this system.

Acknowledgements

The authors are thankful to Inter University Accelerator Centre (IUAC), New Delhi, India for providing financial support in the form of a Project No. 4133 and their permission for providing research facility for this work. Special thanks to Dr. D. Kabiraj target laboratory of IUAC for sample preparation and academic discussions during our work.

References

[1] A. Zaluska, L. Zaluski, J.O. Ström-Olsen, Appl. Phys. A 72 (2001) 157–165.
[2] H. Imamura, K. Masanari, M. Kusuhara, H. Katsumoto, T. Sumi, Y. Sakata, J Alloys Compd. 386 (2005) 211.
[3] M. Zhu, H. Wang, L.Z. Ouyang, M.Q. Zeng, Int. J. Hydrogen Energy 31 (2006) 251.
[4] J. Čermák, L. Král, Int. J. Hydrogen Energy 33 (2008) 7464.
[5] S. Orimo, A. Züttel, K. Ikeda, S. Saruki, T. Fukunaga, H. Fujii, L. Schlapbach, J. Alloys Compd. 293–295 (1999) 437–442.
[6] J. Qu, Y. Wang, L. Xie, J. Zheng, Y. Liu, X. Li, Int. J. Hydrogen Energy 34 (2009) 1910.
[7] W. Lohstroh, R.J. Westerwaal, B. Noheda, S. Enache, I.A.M.E. Giebels, B. Dam, R. Griessen, Phys. Rev. Lett. 93 (2004) 197404.
[8] J.L. Slack, J.C.W. Locke, S.-W. Song, J. Ona, T.J. Richardson, Sol. Energy Mater. Sol. Cell 90 (2006) 485.
[9] T.J. Richardson, J.L. Slack, R.D. Armitage, R. Kostecki, B. Farangis, M.D. Rubin, Appl. Phys. Lett. 78 (2001) 3047.
[10] S.T. Sabitu, G. Gallo, A.J. Goudy, J. Alloys Compd. 499 (2010) 35–38.
[11] K. Higuchi, K. Yamamoto, H. Kajioka, K. Toiyama, M. Honda, S. Orimo, H. Fujii, J. Alloys Compd. 330 (2002) 526–530.
[12] J. Rydén, B. Hjörvarsson, T. Ericsson, E. Karlsson, A. Krozer, B. Kasemo, J. Less-Common Met. 152 (1989) 295–309.
[13] A.J. Du, S.C. Smith, X.D. Yao, G.Q. Lu, J. Am. Chem. Soc. 129 (2007) 10201–10204.
[14] S. Ghosh, A. Ingale, T. Som, D. Kabiraj, A. Tripathi, S. Mishra, S. Zhang, X. Hong, D.K. Avasthi, Solid State Commun. 120 (2001) 445–450.
[15] G.L.N. Reddy, S. Kumar, Y. Sunitha, S. Kalavathi, V.S. Raju, J. Alloys Compd. 481 (2009) 714–718.
[16] Sanjiv Kumar, G.L.N. Reddy, V.S. Raju, J. Alloys Compd. 476 (2009) 500–506.
[17] Y.E. Suyun, O. Liuzhang, Z. Min, Rare Met. 25 (2006) 295.
[18] L.C. Feldman, J.W. Mayer, in: L.C. Feldman, J.W. Mayer (Eds.), Fundamentals of Surface and Thin Film Analysis, North-Holland, New York, 1986, p. 85.
[19] V.K. Mittal, S. Lotha, D.K. Avasthi, Radiat. Effects Defects Solids 147 (1999) 199.
[20] S.P. Singh, P. Srivastava, S. Ghosh, S.A. Khan, G. Vijaya Prakash, J. Phys.: Condens. Mat. 21 (2009) 095010.